Simultaneous acceleration and pitch angle scattering of field-aligned electrons observed by the LEPA on CRRES

G. A. Abel,[1] A. N. Fazakerley, and A. D. Johnstone[2]

Mullard Space Science Laboratory, University College London, Surrey, United Kingdom

Received 1 October 2001; revised 20 March 2002; accepted 26 April 2002; published 3 December 2002.

[1] Using data from the Low Energy Plasma Analyzer we present detailed pitch angle versus energy electron distributions at the time of field-aligned electron events. We present three case studies, as well as the findings of a larger survey of 158 events. These distributions show that electrons are apparently scattered in pitch angle out of field-aligned electron beams observed around 0.1–1 keV. Generally, this pitch angle scattering is accompanied by simultaneous acceleration. As electrons are scattered from the field-aligned beam to pitch angles of ~60°, they typically increase to energies of around 10 keV. The electrons are then seen to scatter to 90° pitch angle with no further change in energy. The observations suggest that this scattering and acceleration takes place near the geomagnetic equator and over a limited range of latitudes. *INDEX TERMS:* 2730 Magnetospheric Physics: Magnetosphere—inner; 2788 Magnetospheric Physics: Storms and substorms; 2716 Magnetospheric Physics: Energetic particles, precipitating; 2720 Magnetospheric Physics: Energetic particles, trapped; 2736 Magnetospheric Physics: Magnetosphere/ionosphere interactions; *KEYWORDS:* substorms, pitch angle distributions, pitch angle scattering, particle acceleration, electron, wave particle interaction

Citation: Abel, G. A., A. N. Fazakerley, and A. D. Johnstone, Simultaneous acceleration and pitch angle scattering of field-aligned electrons observed by the LEPA on CRRES, *J. Geophys. Res.*, *107*(A12), 1416, doi:10.1029/2001JA005090, 2002.

1. Introduction

[2] Field-aligned electrons have been observed in the equatorial regions of the magnetosphere by a range of satellites (ATS-6 [*Parks et al.*, 1977; *Lin et al.*, 1979; *Moore and Arnoldy*, 1982], GEOS-1 [*Borg et al.*, 1978] GEOS-2 [*Kremser et al.*, 1988], SCATHA (P78-2) [*Richardson et al.*, 1981; *Arnoldy*, 1986], and AMPTE/CCE [*Klumpar et al.*, 1988; *Klumpar*, 1993]. However, the observations of field-aligned electron events (FAEs) made with the CRRES spacecraft [*Johnstone et al.*, 1994; *Abel et al.*, 2002] are superior in terms of both angular and energy resolution and coverage.

[3] *Abel et al.* [2002] showed that FAEs are seen associated with substorms and times of enhanced geomagnetic activity and are often seen within 20 min of substorm onset. They showed that the FAEs were only seen outside of the plasmasphere and rarely on the dayside. The occurrence frequency of the events increased with radial distance (to the extent of CRRES' orbit) and peaked either side of midnight at 0400 MLT and 1930 MLT. It was also suggested that the source of the FAEs are the field-aligned beams seen by FAST [*Carlson et al.*, 1998] and other high latitude spacecraft (e.g. Freja [*Boehm et al.*, 1995]). The upcoming electrons beams are an integral part of the magnetospheric/auroral current system. Aurora are seen in the upward current region where electrons are accelerated downward. In the adjacent downward current regions electrons are accelerated out of the ionosphere, and these regions are thought of as the inverse aurora. It is likely therefore that FAEs may play a significant role as carriers of substorm-enhanced field-aligned currents (FACs). Just as the aurora and associated current systems are enhanced during substorms and periods of high geomagnetic activity, so too is the probability of observing an FAE.

[4] The only reported observations (until now) which have suggested that field-aligned electrons are scattered out of counterstreaming beams to larger pitch angles in the region under study are those made with the ATS 6 satellite [*Lin et al.*, 1979; *Moore and Arnoldy*, 1982]. *Lin et al.* [1979] studied three examples and found that the distribution functions could be approximated by the superposition of two Maxwellians following substorm onset. It was found that there was a high temperature (~3 keV) component seen at all pitch angles and a low temperature (~1 keV) beam component seen initially only at small pitch angles (≤30°). After some time passed, the low-temperature component was also seen at large pitch angles. *Lin et al.* [1979] proposed that the beam particles are scattered to larger pitch angles by wave-particle interactions occurring near the equatorial plane.

[5] The scattering of field-aligned beam electrons to larger pitch angles may prove to be an important process. If their source does lie in the ionosphere (as suggested by *Abel et al.* [2002]), then the scattering represents a mechanism by which these particles are trapped in the magnetosphere. In this paper we present detailed energy-pitch angle distributions associated with counterstreaming electrons in the equatorial regions of the magnetosphere. It will be shown that pitch angle scattering takes place from the loss cone toward 90°

[1]Now at British Antarctic Survey, Natural Environment Research Council, Cambridge, United Kingdom.

[2]Deceased 28 May 1999.

0148-0227/02/2001JA005090$09.00

and that it is usually accompanied by acceleration to higher energies. The acceleration of the electrons is a new feature, not reported in observations prior to the CRRES mission.

[6] The acceleration of FAEs seen by LEPA was first reported by *Johnstone et al.* [1996], who undertook an initial study of six events. Unfortunately the study was conducted prior to the discovery of the on-board processing error discussed in section 2 and so the pitch angle energy distributions shown were invalid. Our investigations have expanded the study throughout the lifetime of CRRES, having corrected for the on-board processing error.

2. Instrumentation

[7] The Combined Release and Radiation Effects Satellite (CRRES) operated between July 1990 and October 1991. The spacecraft's highly elliptical orbit took it through a large range of L-shells out to $L = 8$. The spacecraft was oriented such that its spin axis lay in the ecliptic and pointed 12° ahead of the Sun's apparent motion. The nominal spin period of the spacecraft was 30 s. Further details of the satellite and orbit are given by *Johnson and Ball* [1992].

[8] The distributions presented here are constructed using data from the electron sensor of the Low Energy Plasma Analyzer (LEPA). The LEPA consists of two tri-quadrispherical electrostatic analyzers, one configured for electrons and the other for ions. The analyzers are mounted such that the 120° × 5° fan field of view covers angles 30° to 150° with respect to the spacecraft spin axis. This 120° FOV is split into 15 equal anodes each covering 8° × 5°.

[9] Owing to telemetry constraints, not all of the collected data can be returned. For this reason, different telemetry modes were utilized returning different portions of the collected data. LEPA spent most of its lifetime operating in one of two principal telemetry modes. The first returned electron observations for three planar distributions at 8° by 5° resolution, and the second returned electron observations from the whole of the sampled sky at 16° by 22.5° resolution. Full details of the LEPA and its operating modes are given by *Hardy et al.* [1993]. During the early stages of this study (July 1997) an on-board processing error was found. The result of this error was the misidentification of the magnetic field direction and thus the data telemetered down were not the portion of the collected data which were expected. The apparent field direction was mirrored around the spacecraft equator. As a result there was little effect when the magnetic field direction was near perpendicular to the spacecraft spin axis. However, at other times there was a loss of data and errors in the calculation of pitch angles. It has been possible to correct for this error on the ground by performing weighted averages of the returned data over a one spacecraft spin period (30 s), and we have been able to reconstruct full 180° pitch angle distributions for nearly all times during the mission. Pitch angle arrays have been created, with 33 bins, 5.6° wide, covering the range −2.8° to 182.8° A discussion of the on-board processing error and its effects can be found in Appendix A, while full details and details of the pitch angle array construction are given by *Abel* [1999]. The data collected at 16° by 22.5° resolution have proved insufficient to reveal the level of detail required to see the scattering and acceleration features which are the subject of this paper. Thus we have restricted this study to pitch angle distributions constructed from the three planar distributions which can provide the required resolution.

3. CRRES/LEPA Observations of FAEs

[10] In this section we present three case studies which illustrate the various acceleration features seen in FAEs. As discussed in section 2, this study only includes those times when high angular resolution data were returned. LEPA was operated in the required mode for the majority of the time prior to Orbit 614 and occasionally following Orbit 614. Of the 532 FAEs identified by *Abel et al.* [2002] in the LEPA data set, 158 are suitable for the detailed investigation of distributions. While there is a sufficient number of events to allow common features to be identified it must be noted that owing to the nature of the CRRES orbit, this subset of the events covers MLTs only in the range 19:00–08:00 and is biased to post-midnight observations north of the geomagnetic equator.

[11] The three events discussed below have been chosen such that the FAE is the dominant feature in the distributions, i.e., there are no significant electron fluxes other than those associated with the FAE. Many events occur during very active times and other electron populations, such as substorm injected electrons, are also present. During such active times the evolution of the field-aligned electron distributions consistent with the examples shown below can be seen, though less clearly. The three events have been chosen to illustrate the range of characteristics seen, and the first event discussed should be considered typical. Though all three events occur in the morning sector, this is simply due to taking examples from early in the lifetime of CRRES when apogee was so located, and one should not consider the location of the particular events shown here to be typical or special. Similar evolution of the pitch angle distribution associated with FAEs can be seen at all MLTs at which FAEs are seen. In this paper we confine our discussion to the evolution of the electron distributions and not on their relation to substorms and geomagnetic activity (which is discussed in detail by *Abel et al.* [2002]). Two of the events (Orbits 77 and 69) occur within a few minutes of substorm onset, and the other (Orbit 264) occurs within a period of prolonged high geomagnetic activity. In our studies we have found no evidence to suggest any systematic variation in the evolution of FAEs with location (within the constraints of the sampling bias), although there are variations in other features seen in the electron distributions.

3.1. Orbit 77

[12] Figure 1 shows a sequence of energy versus pitch angle plots, each averaged over 1 spin. The color scale of the plots has been allowed to saturate at higher fluxes in order to emphasize certain features. The 88 plots cover the period from 1534 UT to 1618 UT on 26 August 1990, each marked with a time stamp above the plot. During this period CRRES moves from [L = 6.8, 0639 MLT, 15.8° magnetic latitude] to [L = 6.8, 0705 MLT, 16.5° magnetic latitude] and the AE index is in the range 437–956 nT. Each panel is marked with a time stamp giving UT in hours, minutes, and seconds, indicating the start time of the averaging. The time between successive plots is not always exactly 30 s; there are two reasons for this. First, for the purposes of collecting distributions a spin is defined as starting when the magnetic field

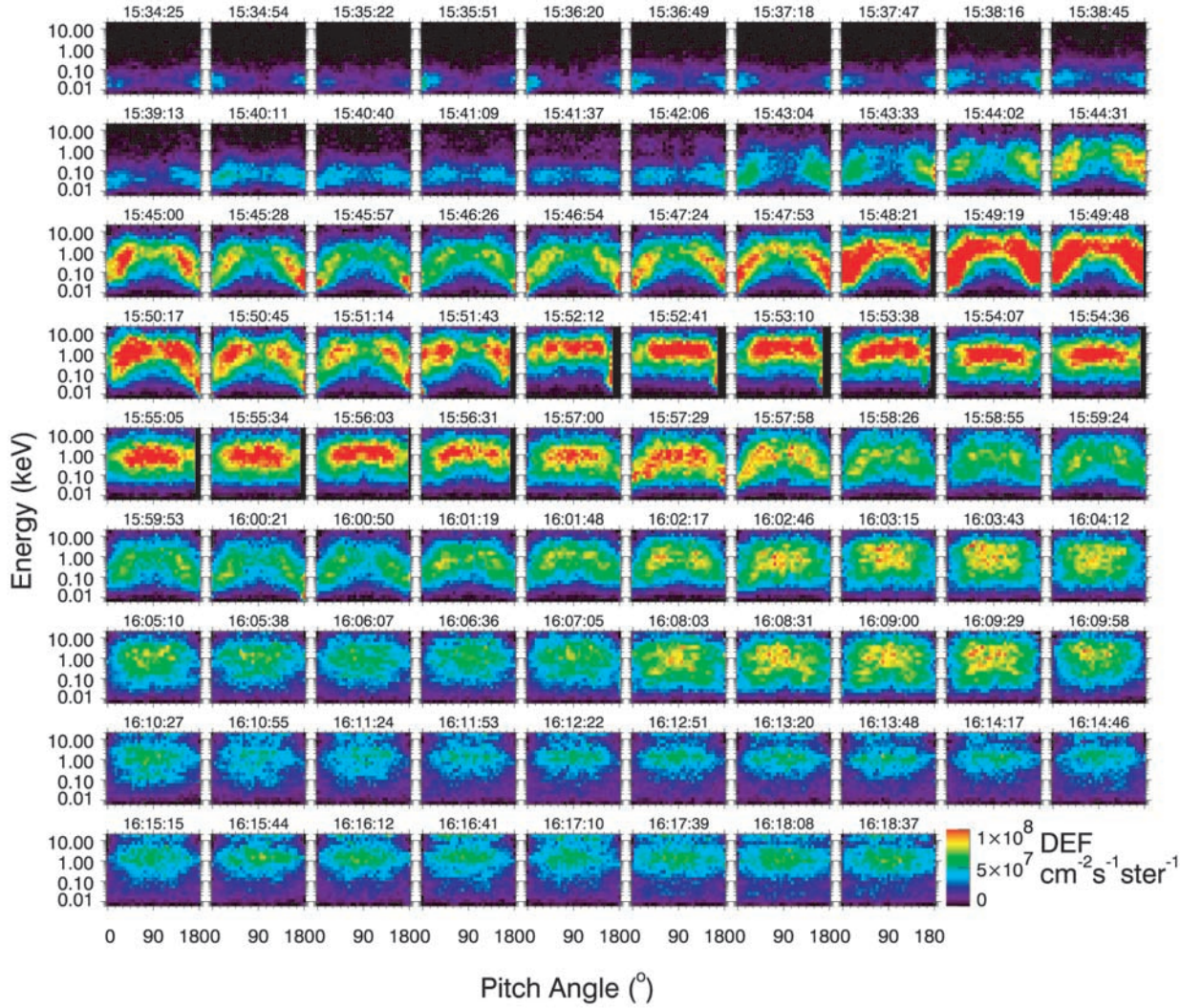

Figure 1. A series of pitch angle energy spectrograms illustrating an FAE on Orbit 77. The FAE lasts from 1543 UT to 1601 UT. The color in each plot indicates the differential energy flux in $cm^{-2}s^{-1}ster^{-1}$ according to the color scale in the lower right corner of the figure. Each panel is marked with a timestamp above it.

direction lies in the field of view of the detector and ending when the magnetic field direction again lies in the field of view of the detector. The magnetic field direction can be quite variable at the time of FAEs (the average change of field direction is over 10° during an FAE) and so a spin as defined here may vary in duration (and start time). The second reason is that occasional gaps in the data mean that a single distribution may occasionally be missing and so the time between successive plots may be around 1 minute.

[13] Weak field-aligned fluxes ($\sim 6 \times 10^7\,cm^{-2}\,s^{-1}\,ster^{-1}$) are seen in most panels in the first row of Figure 1 at energies of 0.01–0.1 keV. By 1540:40 UT there are minima in the field-aligned directions and the peak fluxes are seen at pitch angles of ~20° and ~160° (equatorial pitch angles $\alpha_{eq} \sim 16°$ and ~164°). The main event starts at 1542:06 UT. Initially, field-aligned fluxes are only seen at 180°, though by the next panel they are bidirectional. Over the course of the event (ending at 1551:43) the field-aligned electrons are seen at energies between 10 eV and 800 eV with peak fluxes seen around 100–200 eV, though both this peak energy and the range of energies are seen to vary. Between 1542:06 UT and 1544:31 UT the electrons are seen at larger pitch angles in each successive plot until they cover all pitch angles. Between 0° and 60° (α_{eq} = 45°) and 180° and 120°(α_{eq} = 135°) the energy of the electrons is seen to increase with pitch angle, typically reaching 1 keV, with extremes of up to 10 keV. Between 60° (α_{eq} = 45°) and 90° (α_{eq} = 54°) (and 120°–90°) there is no variation in energy with pitch angle. Following 1552:41 UT the field-aligned electrons disappear, however, substantial fluxes remain above 1 keV, at larger pitch angles, which slowly decrease over the next 30 min.

3.2. Orbit 264

[14] A second event is shown in Figure 2, which is of the same form as Figure 1. This event has been included as an example of FAEs where there is a larger difference in energy between the peak field-aligned fluxes and the 90° fluxes than typically seen in events such as the example shown in Figure 1. While the energy of the electrons may be different from the previous example the key features are the

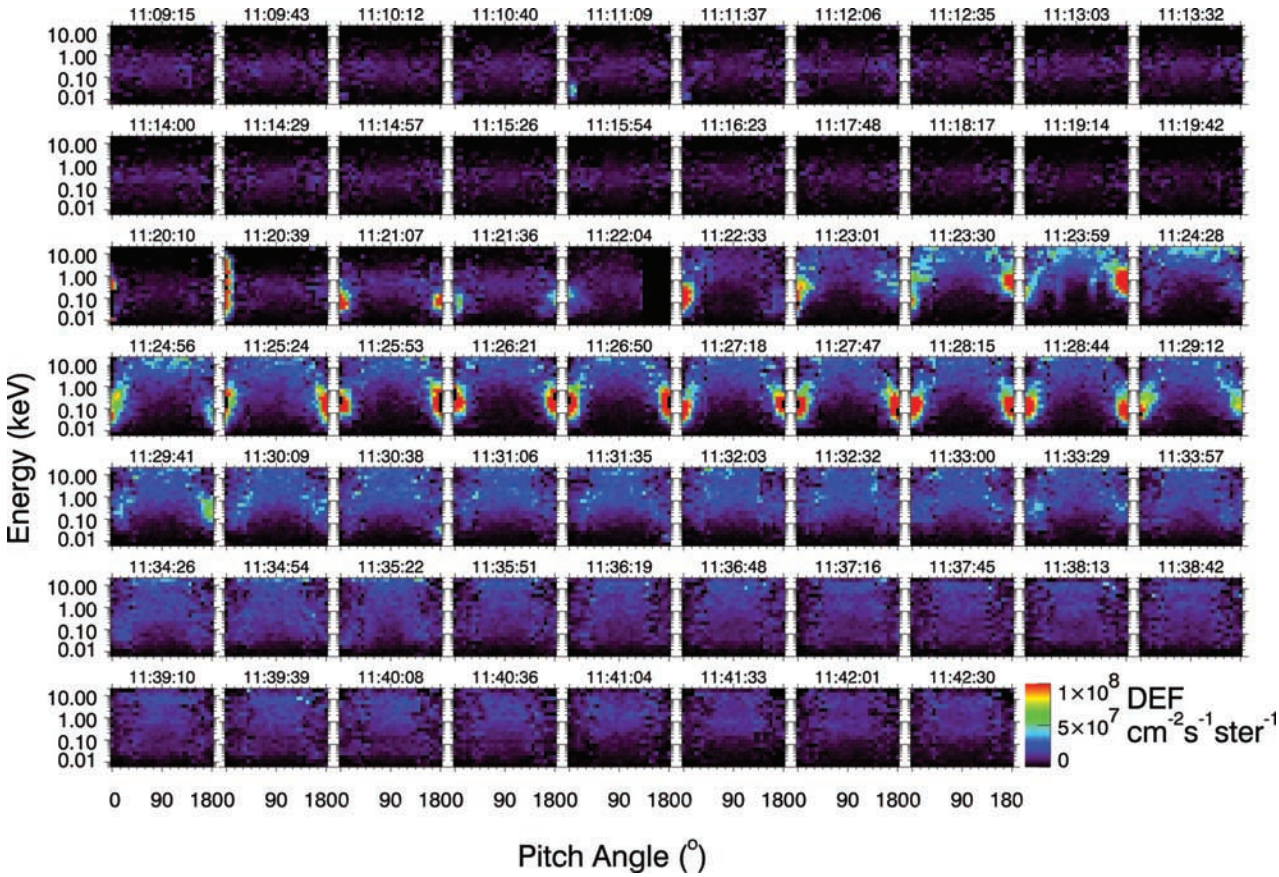

Figure 2. A series of pitch angle energy spectrograms illustrating two FAEs on Orbit 264 at 1050 UT and 1120 UT. The color in each plot indicates the differential energy flux in $cm^{-2}s^{-1}ster^{-1}$, according to the color scale in the lower right corner of the figure.

same. Figure 2 covers the time period 1109 UT to 1142 UT on 11 November 1990, during which time CRRES moves from [L = 8.1, 0328 MLT, 25.6° magnetic latitude] to [L = 7.9, 0347 MLT, 24.8° magnetic latitude]. During this period the AE index is in the range 242–677 nT.

[15] The first signs of the event can be seen in the panel marked 1120:10, where field-aligned fluxes care only seen at 0°. In the next panel (1120:39) these fluxes cover almost the entire energy range of LEPA, still only at 0°. The next panel shows the first signs of particles at 180°, with the electrons at 0° and 180° covering the energy range 60–600 eV. The two beam populations at the 0° and 180° are often seen at different energies in a single panel (e.g. panels 1121:30, 1123:30, 1123:59, and 1129:12). From 1122:04 UT enhanced electron fluxes are seen at increasingly large pitch angles until 1123:59 UT when they are seen at 90° (α_{eq} = 32°). The 90° electrons are seen to extend above the highest energies sampled by LEPA (30 keV), being an order of magnitude more energetic than those seen in Figure 1. As with the example in Figure 1 we again see an increase in energy with pitch angle of the enhanced electron fluxes over a limited pitch angle range (in this case 0–45° (α_{eq} = 22°) and 180–135°), though in this example the gradient is steeper.

3.3. Orbit 69

[16] In a few cases, the field-aligned electrons and those seen at 90° appear to have the same or very similar energies. One such case occurs on Orbit 69 and is shown in Figure 3. The plate covers the period 1011 UT to 1052 UT on 23 August 1990. During this period CRRES moves from [L = 7.3, 0742 MLT, 23.0° magnetic latitude] to [L = 7.0, 0810 MLT, 24.7° magnetic latitude], and the AE index is in the range 636–1653 nT.

[17] A short duration event can be seen on this orbit in the first row of panels of the energy versus pitch angle plots in Figure 3 at 1012:27. The main event starts in the panel marked 1016:46 as weaker field-aligned fluxes but grows to strong fluxes in the panel marked 1018:12. The strong fluxes of counterstreaming electrons remain evident through to 1038:52 (with the exception of the two panels marked 1023:00 and 1023:29). Again we see enhanced electron fluxes initially only at small pitch angles and later across all pitch angles. However, in this example the 90° (α_{eq} = 43°) electrons are seen at the same energy (0.01–0.1 keV) as the field-aligned electrons.

3.4. General Features

[18] Though in some events, such as the one illustrated in Figure 3, the enhanced electron fluxes at 90° are seen at the same energy as the field-aligned electrons, in the majority of the events lasting longer than a few minutes (and many of the shorter ones) the 90° electrons are observed at higher energies as in the first two examples given above. Of the 158 events for which the pitch angle data have been studied,

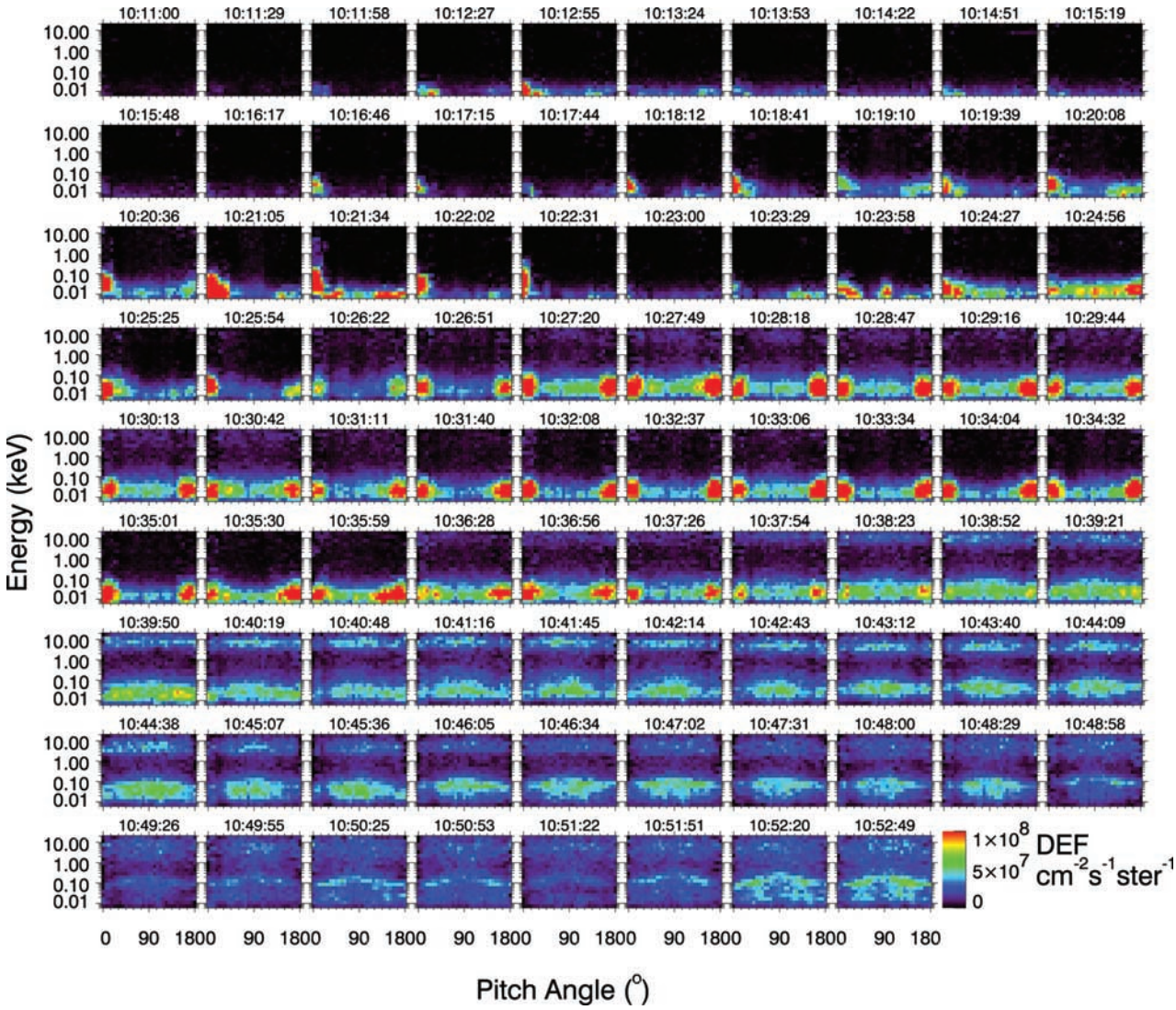

Figure 3. A series of pitch angle energy spectrograms illustrating three FAEs on Orbit 69. The first FAE is in progress at start of the time period shown and the second and third start at 1012 UT and 1018 UT, respectively. The color in each plot indicates the differential energy flux in $cm^{-2}s^{-1}ster^{-1}$ according to the color scale in the lower right corner of the figure.

63% had 90° enhanced electrons at higher energy than the field-aligned electrons, 3% had 90° enhanced electrons at the same energy as the field-aligned electrons, and 14% showed no enhancement of the 90° electron fluxes. In 20% of events the situation is confused by the presence of higher energy electron populations and it is not clear what enhancements if any are associated with the FAE.

[19] The general ordering of the events, illustrated in Figure 4, is always the same. First we see the bidirectional field-aligned beams (a) confined to within ~10–15° of the field direction. Enhanced electron fluxes are then seen at increasing pitch angles (b). These enhanced fluxes are seen to increase in energy with increasing pitch angle. The enhanced fluxes then spread to 90° with energy constant with pitch angle (c). Finally, the beams disappear and the fluxes slowly decrease (d). We do not always see the whole picture and may miss the beginning or end stages of the event, and sometimes the distribution can hop between stages. The fact that we only see this process in the order shown in Figure 4, independent of whether the spacecraft is outbound or inbound, implies that what we see is not due to a consistent spatial organization but rather a temporal effect.

4. Discussion

[20] We interpret our observations, similarly to *Lin et al.* [1979], as a scattering process. The field-aligned beams, which originate below the spacecraft [*Abel et al.*, 2002], act as a source population. Electrons are scattered out of the beams to larger pitch angles. Between 0° and ~60° the electrons undergo simultaneous acceleration and pitch angle scattering (Figure 4b). We shall refer to this as the acceleration leg of the scattering process. Between ~60° and 90° the electrons are scattered in pitch angle alone with no detectable change in energy. Once the source population has been removed, i.e., after the disappearance of the field-

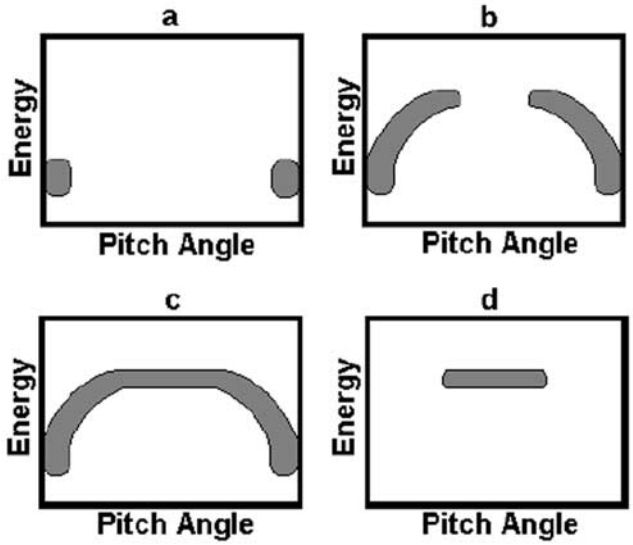

Figure 4. The general ordering of the process of acceleration/scattering of FAEs seen by CRRES. Panels are the same as those in Figures 1, 2, and 3.

aligned beams, the electron fluxes decrease presumably through diffusion into the loss cone. As we discussed above, there are some events where no acceleration is seen, though these are unusual.

[21] The fact that the field-aligned beams are often seen at different energies may indicate that the two beams have separate sources and are not just mirroring trapped populations, though some component of a mirroring population is apparently present in most panels. An alternative explanation is that within half a spin period, CRRES moves from a lower energy beam to one with a higher energy and the data processing combines these observations as apparently different energy beams at 0° and 180°.

[22] Some further insight into the mechanism responsible for the acceleration can be gained from studying the distributions in velocity space using coordinates perpendicular and parallel to the magnetic field. We use the FAE during Orbit 77 as a typical example.

[23] Figure 5 shows the data from a single panel of Figure 1 in $v_\perp$ versus $v_\parallel$ coordinates when the scattered electrons cover all pitch angles. Figure 5a shows the data in differential energy flux (as in Figure 1) while Figure 5b shows the data plotted in terms of phase space density. By plotting the data in differential energy flux we can easily identify the accelerated and pitch angle scattered electrons. In contrast, the phase space density plot is dominated by the fall-off of the distribution function with increasing energy but allows a more physical interpretation. While phase space density is the quantity which is conserved during scattering processes, at any particular energy differential energy flux and phase space density are directly proportional to one another. It is this relationship which allows us to identify the enhanced electrons at any one particular energy and thus the scattered population. The black lines on each plot are intended to represent the scattering path and have been identified by eye from Figure 5a. The electrons which appear in the loss cone have parallel velocities in the range $1 \times 10^7\ \mathrm{ms}^{-1} < v_\parallel < 3 \times 10^7\ \mathrm{ms}^{-1}$ (300 eV $< E <$ 2.6 keV). The electrons are scattered out of the field-aligned beam and accelerated both perpendicular and parallel to the magnetic field with an overall change in velocity of around $3\text{–}4 \times 10^7\ \mathrm{ms}^{-1}$. At higher energies the electrons continue increasing in perpendicular velocity while equally decreasing in parallel velocity, in other words they are scattered in pitch angle (toward 90°) with little or no change in total velocity. The white line on Figure 5 is plotted at a constant velocity as a guide.

[24] The main feature to note from Figure 5b is that the distribution function decreases along the scattering path indicated by the black lines away from 0°. This is typical of a diffusion process, during which the net motion of a scattered particle population is from regions of high phase space density to regions of lower phase space density [*Thorne and Horne*, 1996]. Ignoring the highlighted scattering path we see at low energies there is a negative gradient in phase space density away from the field aligned direction and toward higher energies and as such one would expect a net motion of electrons to larger pitch angles and higher energies. At higher energies there is a negative gradient toward the loss cone, which is likely to result in the diffusion and loss by precipitation of electrons following the acceleration event.

[25] We suggest that the source of the scattering resulting in the simultaneous pitch angle and energy diffusion process may be wave-particle interactions with either whistler mode waves or ECH waves. We have tried to find a statistical link between the acceleration seen in the LEPA data and the wave power of the whistler mode and ECH waves measured by the Plasma Wave Experiment (PWE) on CRRES (employing a similar technique to that of *Meredith et al.* [2000a]). However, no such link has been found. There are reasons why scattering may take place preferentially at different locations, such as the confinement of ECH waves (and to a lesser extent whistler mode waves) to near the geomagnetic equator, and so CRRES may not observe the waves responsible. Even when restrictions were placed on the magnetic latitude and MLT of the observation sites (as we might not expect to see correlations outside of an interaction region) no connections could be made. The situation is further complicated

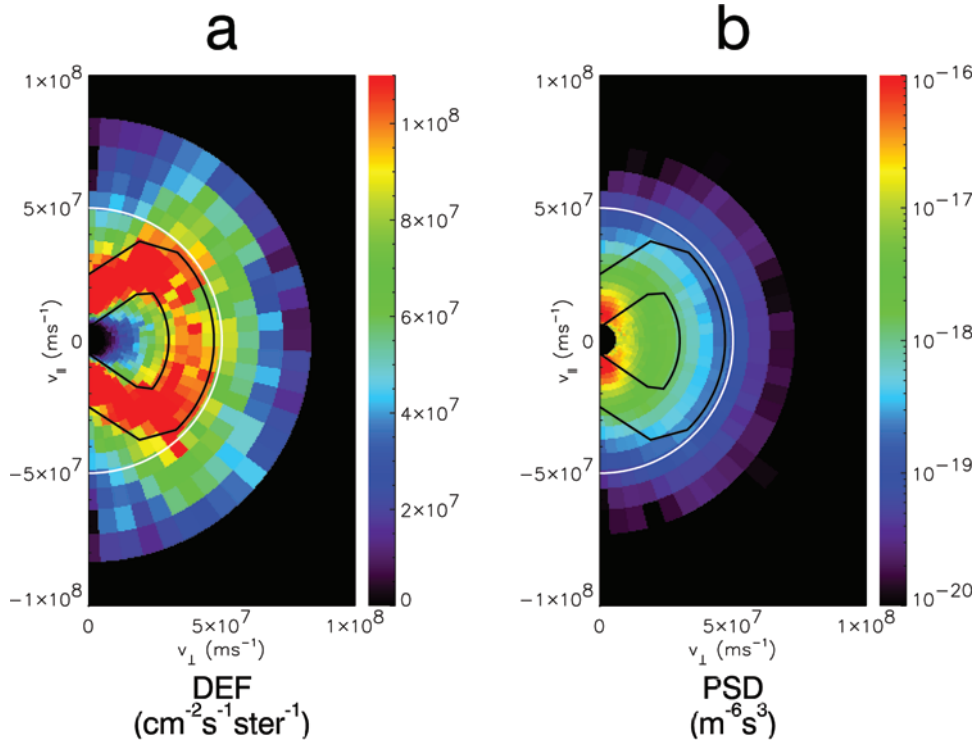

Figure 5. (a) The 1549:19 UT panel from Figure 1 plotted in velocity space. The color scale indicates the differential energy flux (note linear scale). The white line indicates a contour of constant speed, $v = 5 \times 10^7$ ms^{-1}, and the black lines indicate the edges of the scattering path (identified by eye). (b) The same data plotted in terms of phase space density (note logarithmic color scale). The white and black lines are the same as those plotted in Figure 5a.

by the fact that phase velocity of many plasma waves is dependent on the plasma density and so too is the nature of the resonant interactions with electrons. It is likely that a combination of different wave intensities and plasma densities give rise to the range of scattering characteristics we observe. Unfortunately, during the active times when FAEs are normally observed it is not possible to make a useful estimate of the electron density from the upper hybrid emissions seen with the PWE.

[26] It is worth noting that the observed diffusion path highlighted in Figure 5a is different from the theoretical diffusion path suggested by *Summers et al.* [1998], for resonant interactions between electrons and whistler mode waves. The theoretical diffusion paths do not allow simultaneous increases in $v_\perp$ and $v_\parallel$. However, this does not necessarily preclude whistler mode waves from producing the observed diffusion, as the analysis of *Summers et al.* [1998], was based on the cold plasma dispersion relation, and the diffusion curves may change somewhat if a more realistic dispersion relation (including the beam populations) were used. To our knowledge no work has been published detailing the characteristic diffusion path for resonant interactions between electrons and ECH waves, however, the theoretical study by *Lyons* [1974] does show comparable diffusion coefficients for pitch angle and velocity diffusion. While this is encouraging and suggests that ECH waves could give rise to the process seen here, the calculations of *Lyons* [1974] do depend on the distribution function and so may not be directly comparable.

[27] Another possible source of acceleration is neutral sheet acceleration such as that outlined by *Lyons and Speiser* [1982]. However, neutral sheet acceleration is unlikely to produce the observed features in the examples shown here as neutral sheet acceleration results in equal changes in velocity between ions and electrons. In the simulations presented by *Lyons and Speiser* [1982] the velocity change of 1 keV ions was $\sim 5 \times 10^5$ ms^{-1} and preferentially in the field aligned direction. This is quite different from the $\sim 3 \times 10^7$ ms^{-1} change in velocity we observe in the electrons peaking at $\sim 60°$ pitch angle.

[28] There is a question as to whether the diffusion path seen arises as the result of two processes rather than a single process as we have discussed up until now, i.e., one process causes the simultaneous pitch angle scattering and acceleration (up to pitch angles of $\sim 60°$) and another causing the pitch angle scattering with no change in energy (from $\sim 60°$ to $90°$ pitch angle). In fact, acceleration of electrons perpendicular to the field direction occurring off of the equator could produce the acceleration leg of the scattering path (see Figure 6). The fact that we always see the scattering in pitch angle only extending from the ends of the acceleration leg of the scattering path and not from all along it is suggestive of a single process. However, if a second process becomes dominant above a certain energy, pitch angle, or $v_\perp$ (though not $v_\parallel$), the scattering may manifest itself in such a way. If the pitch angle scattering with no change in energy were to be due to a separate process we would expect the electrons to diffuse toward $90°$ and toward the loss cone. In fact the

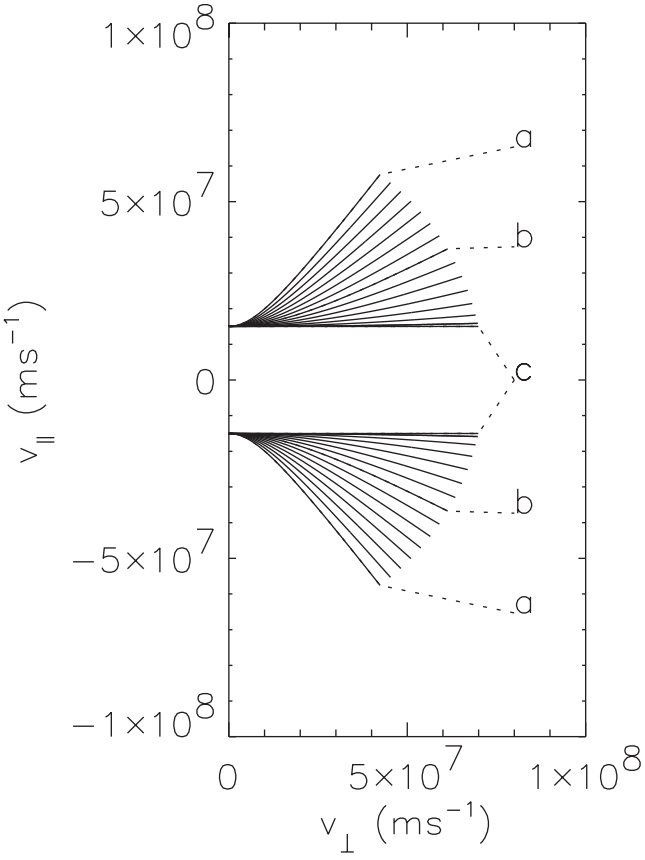

Figure 6. This figure illustrates how scattering over a range of latitudes could result in a spread in the observed scattering path. For purpose of illustration we have taken a monoenergetic beam population at $v_{\|} = \pm 1.5 \times 10^7$ ms^{-1} and $v_{\perp} = 0$ and considered the electrons scattering in $v_{\perp}$ only at one specific magnetic latitude. Each line represents electrons scattered from the beam population at different magnetic latitudes (lines are shown for each 2° of magnetic latitude) as seen at the geomagnetic equator. With the exception of the scattering itself, the electrons are assumed to move adiabatically; that is, line **a** shows the path at the geomagnetic equator occupied by the scattered beam electrons when they are scattered in $v_{\perp}$ at 30° magnetic latitude. Note that this line is very similar to the scattering and acceleration leg of the scattering path seen in Figure 5. Similarly, line **b** shows the path at the geomagnetic equator occupied by the scattered beam electrons when they are scattered in $v_{\perp}$ only at 14° magnetic latitude. Line **c** shows the scattering path of the beam electrons scattered at the equator. From this we can clearly see that scattering over a large range of latitudes would result in a broad observed scattering path. Note that the scattering in $v_{\perp}$ is used only as a simply illustration and is not supposed to be representative of the scattering path which is the topic of this paper.

gradient in phase space density is higher toward the loss cone, and so one would expect a higher net transport of electrons toward the loss cone. It may be that electrons are scattered toward the loss cone, but owing to the removal of electrons by precipitation no net enhancement is seen. While there are both indications of either two separate processes or a single process at work, neither case is clear. It must also be considered that a single process could be the result of electrons interacting with both ECH and whistler mode waves across all energies.

[29] In nearly all FAEs we see a clearly defined, fairly narrow diffusion path in velocity space (by narrow we mean that the width of the diffusion path in velocity space is similar to the width in velocity space of the field-aligned beams). This implies that the scattering takes places over a small range of magnetic latitudes. If the scattering were taking place over a wide range of latitudes, given that the scattering follows a characteristic path, we would expect spread to be introduced to the observed scattering path (see Figure 6). It is possible that the effect of scattering at different latitudes may be counteracted by an equal and opposite change in scattering path; however, this is unlikely. In fact, in the scattering path presented by *Summers et al.* [1998], the variation of scattering path with magnetic latitude works to exaggerate this effect. Also the fact that in most cases we see electrons scattered to 90° (including times when CRRES is on the geomagnetic equator) implies that this scattering region must be located at the equator.

5. Conclusions

[30] We have shown for the first time that the electrons which form the counterstreaming beams often seen in the equatorial regions of the inner magnetosphere are scattered in pitch angle while simultaneously being accelerated. This pitch angle scattering is common in the FAEs seen with the LEPA on CRRES. The characteristics of the scattering are (1) The scattering from 0° to ~60° pitch angle is accompanied by acceleration from energies <1 keV to typically around 10 keV. (2) The scattering from ~60° to 90° pitch angle takes place with little or no change in energy. (3) Occasionally, scattering is seen without acceleration across all pitch angles. (4) The scattering process is diffusion like insofar as there is a negative gradient in phase space density along the diffusion path. (5) The scattering takes place near the geomagnetic equator over a limited range of latitudes. Wave particle interactions can produce pitch angle and energy scattering of electrons. It is likely that whistler mode waves, ECH waves, or a combination of the two are responsible.

Appendix A: Correction to On-board Processing Error

[31] The correction to the electron pitch angle distributions is not a straightforward matter and depends very much on the source of the magnetic field direction data and the way in which the distributions are calculated. Before discussing the error it is worth noting two facts: First, this error has little effect when the magnetic field direction is close to perpendicular to the spacecraft spin axis, as is normally the case near the geomagnetic equator during quiet times, and second, the effect is most apparent when the electron distribution contains distinct field-aligned features (hence the discovery during this study).

[32] The essential problem is that the information regarding the magnetic field direction which was fed into the LEPA and used on-board for the identification of the portions of the collected data to be included in the telemetry,

was somehow misinterpreted. The effect resulted in LEPA using an apparent field direction which was the actual field direction mirrored about the plane perpendicular to the spacecraft spin axis. The result of this error is that while the ''90°'' and ''loss cone'' telemetry distributions are correctly identified the ''symmetry plane'' telemetry distribution is not (the various telemetry distributions are fully described by *Hardy et al.* [1993]. The ''symmetry plane'' distribution does not represent a 180° pitch angle distribution as expected and in extreme cases represents only pitch angles close to 90°. Included in the LEPA telemetry, along with the electron data, was the number of the detector zone in which the apparent field direction lay. This number can be used in conjunction with a look-up table to identify which detector zones were identified and collected as the ''symmetry plane.'' If pitch angle distributions are calculated directly using a magnetic field direction calculated using data taken from the magnetometer telemetry, and provided that no assumptions are made about the collection of ''symmetry plane'' data (i.e., the actual zones collected are calculated from the look-up table), the distributions should be correct. However, many pitch angle distributions, such as those presented by *Johnstone et al.* [1996], are calculated using the information in the LEPA telemetry on which zone contained the magnetic field direction. If this is the case the detector zones which were included in the telemetry as the ''symmetry plane'' need to be identified as usual using the apparent field direction, and then pitch angle distributions calculated using the real field direction (i.e., the apparent direction mirrored about the plane perpendicular to the spacecraft spin axis). Similar treatment should also be applied to the ''3-D'' telemetry distributions which are not used in this study. Please note that the work of *Meredith et al.* [1999, 2000a, 2000b] has taken this correction into account.

[33] **Acknowledgments.** GAA would like to acknowledge a PPARC studentship which funded part of this work.

[34] Michel Blanc and Lou-Chuang Lee thank two reviewers for their assistance in evaluating this paper.

References

Abel, G. A., Field aligned electron distributions in the inner magnetosphere, Ph.D. thesis, University College, London, September 1999.

Abel, G. A., A. N. Fazakereley, and A. D. Johnstone, Statistical distributions of field-aligned electron events in the near equatorial magnetosphere observed by the LEPA on CRRES, *J. Geophys. Res.*, *107*(AX), doi:10.1029/2001JA005073, 2002.

Arnoldy, R. L., Fine structure and pitch angle dependence of synchronous orbit electron injections, *J. Geophys. Res.*, *91*, 13,411–13,421, 1986.

Borg, H., L. A. Holmgren, B. Hultqvist, F. Cambou, H. Reme, and A. Bahnsen, Some early results of the keV plasma experiment on GEOS-1, *Space Sci. Rev.*, *22*, 511–535, 1978.

Hardy, D. A., D. M. Walton, A. D. Johnstone, M. F. Smith, M. P. Gough, A. Huber, J. Pantazis, and R. Burkhardt, Low Energy Plasma Analyzer, *IEEE Trans. Nucl. Sci.*, *40*, 246–251, 1993.

Johnson, M. H., and J. K. Ball, Combined Release and Radiation Effects Satellite (CRRES): Spacecraft and mission, *J. Spacecraft Rockets*, *29*, 556–563, 1992.

Johnstone, A. D., N. J. Flowers, and R. Liu, Observations in the equatorial region of the field aligned electron and ion distributions in the energy range 100 eV to 5 keV associated with substorm onsets, paper presented at Second International Conference on Substorms, Geophys. Inst., Fairbanks, Alaska, 1994.

Johnstone, A. D., S. Szita, N. J. Flowers, and N. P. Meredith, Observations of Particle Injection From CRRES, paper presented at Third International Conference on Substorms, Eur. Space Agency, Versailles, France, 1996.

Klumpar, D. M., J. M. Quinn, and E. G. Shelley, Counterstreaming electrons at the magnetic equator near 9 R_E, *Geophys. Res. Lett.*, *15*, 1295–1298, 1988.

Klumpar, D. M., Statistical distributions of the auroral electron albedo in the magnetosphere, *Auroral Plasma Dynamics*, *Geophys. Monogr. Ser.*, vol. 80, edited by R. L. Lysak, pp. 163–171, AGU, Washington, D.C., 1993.

Kremser, G., A. Korth, S. L. Ullaland, S. Perraut, A. Roux, A. Pedersen, R. Schmidt, and P. Tanskanen, Field aligned beams of energetic electrons (16 keV $\leq$ E $\leq$ 80 keV) observed at geosynchronous orbit at substorm onsets, *J. Geophys. Res.*, *93*, 14,453–14,464, 1988.

Lin, C. S., G. K. Parks, S. DeForest, and C. E. McIlwain, Temperature characteristics of electron beams and ambient particles, *J. Geophys. Res.*, *84*, 2651–2654, 1979.

Lyons, R. L., Electron diffusion driven by magnetospheric electrostatic waves, *J. Geophys. Res.*, *79*, 575–580, 1974.

Lyons, R. L., and T. W. Speiser, Evidence for current sheet acceleration in the geomagnetic tail, *J. Geophys. Res.*, *87*, 2276–2286, 1982.

Meredith, N. P., A. D. Johnstone, S. Szita, R. B. Horne, and R. R. Anderson, ''Pancake'' electron distributions in the outer radiation belts, *J. Geophys. Res.*, *104*, 12,432–12,444, 1999.

Meredith, N. P., R. B. Horne, A. D. Johnstone, and R. R. Anderson, The temporal evolution of electron distributions and associated wave activity following substorm injections in the inner magnetosphere, *J. Geophys. Res.*, *105*, 12,907–12,917, 2000a.

Meredith, N. P., A. D. Johnstone, S. Szita, R. B. Horne, and R. R. Anderson, An investigation into the roles of ECH and whistler mode waves in the formation of ''pancake'' electron distributions using data from the CRRES satellite, *Adv. Space Res.*, *25*, 2339–2342, 2000b.

Moore, T. E., and R. L. Arnoldy, Plasma pitch angle distributions near the substorm injection front, *J. Geophys. Res.*, *87*, 4405–4417, 1982.

Parks, G. K., C. S. Lin, B. H. Mauk, S. DeForest, and C. E. McIlwain, Characteristics of magnetospheric particle injection deduced from events observed on August 18, 1974, *J. Geophys. Res.*, *82*, 5208–5214, 1977.

Richardson, J. D., J. F. Fennel, and D. R. Croley Jr., Observations of field aligned ion and electron beams from SCATHA (P78-2), *J. Geophys. Res.*, *86*, 10,105–10,110, 1981.

Summers, D., R. M. Thorne, and F. Xiao, Relativistic theory of wave-particle resonant diffusion with application to electron acceleration in the magnetosphere, *J. Geophys. Res.*, *103*, 20,487–20,500, 1998.

Thorne, R. M., and R. B. Horne, Whistler absorption and electron heating near the plasmapause, *J. Geophys. Res.*, *101*, 4917–4928, 1996.

G. A. Abel, British Antarctic Survey, High Cross, Madingley Road, Cambridge CB3 0ET, UK. (gaab@bas.ac.uk)

A. N. Fazakerley, Mullard Space Science Laboratory, University College London, Holmbury St. Mary, Dorking, Surrey RH5 6NT, UK. (anf@mssl.ucl.ac.uk)